



Factorial design analysis for biosorption of Reactive Red-84 dye using fermentation spent waste biomass, biosorbent regeneration and desorbed dye photo-degradation using TiO₂ nanoparticles

Nour Sh. El-Gendy^{a,*}, Salem S. Abu Amr^b, Radwa A. El-Salamony^a, Hussein N. Nassar^a

^aEgyptian Petroleum Research Institute, Nasr City, Cairo 11727, Egypt, emails: nourepri@yahoo.com (N.Sh. El-Gendy), radwa2005@hotmail.com (R.A. El-Salamony), hessen_nasar@hotmail.com (H.N. Nassar)

^bSchool of Civil Engineering, Engineering Campus, Universiti Sains Malaysia, 14300 Nibong Tebal, Penang, Malaysia, email: sabuamr@hotmail.com (S. S. Abu Amr)

Received 16 April 2014; Accepted 18 September 2014

ABSTRACT

In this work, factorial design analysis based on central composite design of experiments was employed to study the effect of process parameters for biosorption of Reactive Red-84 dye onto bioethanol fermentation spent waste biomass of *Saccharomyces cerevisiae*. Factorial experiments with five factors: mixing rate rpm, incubation period h, process temperature °C, initial dye concentration mg/L and biosorbent dosage wt% (w/v) at three levels were conducted. A highly statistically significant quadratic model at 95% confidence level ($p < 0.0001$, R^2 0.9120 and R^2_{adj} 0.8519) was developed to characterize the influence of the different considered variables on biosorption efficiency. Response surface methodology was employed to optimize the process, recording maximum biosorption % of ≈62% (51.67 mg/g) at 90 rpm, 13 h, 15 °C, 100 mg/L and 0.6%, respectively. Approximately 95% of adsorbed dye was desorbed by elution with NaOH solution of pH 9 and the regenerated biosorbent was employed for four successive cycles. TiO₂ nanoparticles 6–15 nm were prepared and used for photo-catalytic degradation of desorbed dye solution. The proposed integrating biosorption and photo-catalytic degradation process results in no secondary pollution in the form of any concentrated wastes, which is an important environmental aspect.

Keywords: Biosorption; Response surface methodology; Photo-catalytic degradation; Reactive Red-84; TiO₂ nanoparticles

1. Introduction

Wastewater contaminated with dyestuffs in industrial effluents is one of the major challenges faced by environmental sector. Reactive group of azo dyes is

mostly used in dyeing, due to their superior fastness to the applied fabric, high photolytic stability and recalcitrant to microbial degradation. Many synthetic azo dyes and their metabolites are toxic, carcinogenic and mutagenic, leading to potential health hazard [1]. In general, the treatment of dye-containing effluents is being undertaken by biological, adsorption, membrane,

*Corresponding author.

coagulation–flocculation, oxidation–ozonation and advanced oxidation processes (AOPs) [2]. AOPs have been developed to degrade the non-biodegradable contaminants of drinking water and industrial effluents into harmless species (e.g. CO₂, H₂O, etc.). In recent years, AOPs using titanium dioxide (TiO₂) have been effectively used to detoxify recalcitrant pollutants present in industrial wastewater [3–6]. TiO₂ has singular characteristics that made it an extremely attractive photo-catalyst: high photo-chemical reactivity, high photo-catalytic activity, low cost, stability in aquatic systems and low environmental toxicity [7]. A wide variety of biomass including algae, bacteria, fungi and yeast are capable for removing broad range of dyes from aqueous effluents, owing to their special surface properties, high selectivity, efficiency, cost effectiveness, abundant availability and environmental acceptability [8–10]. However, how to deal with dye-loaded biosorbents is still a problem to be solved. In order to overcome this problem and lower the cost of biosorption process, the biosorbent regeneration step should be done. Efficient regeneration can be done by alkali or acid solution as eluent [11,12]. But these regeneration methods leave concentrated solutions of dyes, which bring a secondary pollution to the environment that should be eliminated.

In this study, Reactive Red-84 (RR-84) azo dye was selected as pollutant due to its recalcitrant stability. The selected biosorbent is bioethanol fermentation spent waste biomass of *Saccharomyces cerevisiae*, in an aspect of reuse of one of the waste by-products in bioethanol production process, to treat industrial wastewater effluent, in a cost effective process. Factorial design of experiments and response surface methodology (RSM) were employed to optimize the biosorption process as they are faster for gathering experimental research results than the rather conventional, time consuming one-factor-at-a-time approach. TiO₂ nanoparticles were prepared and their photo-catalytic degradation capability on the recalcitrant RR-84 azo dye obtained from the regeneration of biosorbent was investigated in order to overcome the problem of concentrated wastes.

2. Materials and methods

2.1. Biosorbent

Bioethanol fermentation spent waste biomass, *S. cerevisiae*, obtained from Petroleum Biotechnology Lab, Egyptian Petroleum Research Institute was used in this study.

The biomass was washed three times with distilled water, dried overnight at 60°C, then grinded in a

mortar, sieved to constant size (0.07–0.08 mm) and stored for further use.

2.2. Adsorbate

The dye used in this study was C.I. Reactive Red-84 (Reactive Red PW-6G or Lanazol Red-6G), a single azo-class dye, and was purchased from Ciba Specialty Chemicals Inc. It is used for wool fibre, tops, scattered wool dyeing, also can be used for wool, silk fabric printing [C.I. number: 13429, molecular formula: C₂₆H₁₉BrN₄Na₂O₉S₃, molecular weight: 753.53, IUPAC name: disodium 6-amino-5-[4-[(2-bromo-1-oxoallyl) amino]-2-[(4-methyl-3-sulphonatophenyl) sulphonyl] phenyl] azo]naphthalene-2-sulphonate. The structure of Reactive Red-84 (RR-84) is illustrated in Fig. 1.

A stock solution of RR-84 with a concentration of 200 mg/L was prepared in distilled water, which was further diluted according to the experimental conditions.

2.3. Analysis of dye

The λ_{\max} 485 nm of RR-84 was determined on a double-beam JASCO UV/Vis/NIR spectrophotometer model V-570 (JASCO Analytical instruments, 8649 Commerce Drive, Easton, Maryland 21601-9903, USA). Standard curve for different concentrations of the dye solution (200–2.5 mg/L) was established.

2.4. Batch biosorption experiments

Each batch adsorption experiment was conducted by contacting 50 mL (pH 7) of different initial concentrations of RR-84 (adsorbate) with known dose

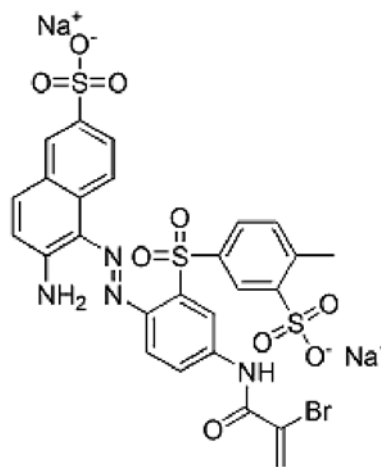


Fig. 1. Chemical structure of Reactive Red-84.

of dried biomass as an adsorbent in 250 mL Erlenmeyer flasks closed with PARAFILM “M” to prevent evaporative loss and placed in a rotary shaking incubator set at different speeds and temperatures according to the experimental conditions. Adsorbent was separated from the solution at predetermined time intervals by centrifugation at 2,000 rpm for 15 min, and then collected for the regeneration experiments. The absorbance of the supernatant solution at 485 nm was measured to determine the residual dye concentration and to calculate the percentage of dye removal. Negative controls (with no biosorbent) were carried out to ensure that any sorption effect of dye onto the wall of the conical flasks is ruled out. The dye concentration of the control was used as the initial concentration (C_0 mg/L) for calculations of dye removal using the following equation:

$$\text{Dye removal} = \left(\frac{C_0 - C_t}{C_0} \right) \times 100 \quad (1)$$

where C_t mg/L is the residual dye concentration at different time intervals (t , h). All experiments were conducted in triplicates and listed data are the average of the obtained results.

2.5. Factorial design of experiments

RSM was used to optimize and investigate the influence of different process variables of the batch biosorption process. The central composite design (CCD) was applied. The experimental runs were carried out according to a 2^5 full factorial design for five independent variables: mixing rate (A , rpm), incubation period (B , h), process temperature (C , °C), initial dye concentration (D , mg/L) and biosorbent dosage (E , % w/v), with low (−1) and high (+1) levels. The total number of experiments is given by the following formula: $[50 = 2^k + 2(k) + 8]$, where k is the number of independent variables ($k = 5$), this includes 32 factorial point from 42 full factorial CCD augmented with eight replicates at the centre point to assess the pure error. The response selected was the percentage dye removal. The levels were selected, based on preliminary study results. The design factors with low (−1), high (+1) and centre (0) levels for the experimental design are listed in Table 1.

2.6. Statistical analysis

Once the experiments were performed, the next step was to perform a response surface experiment to

Table 1

Experimental range and levels of independent process variables for RR-84 removal

Independent variables	Range and levels		
	−1	0	+1
Mixing rate (A , rpm)	50	0	100
Incubation period (B , h)	4	12	20
Process temperature (C , °C)	15	25	30
Initial dye concentration (D , mg/L)	100	150	200
Biosorbent dosage (E , % w/v)	0.2	0.4	0.6

produce a prediction model to determine curvature, detect interactions among the design factors (independent variables) and optimize the process, that is, determine the local optimum independent variables with high biosorption percentage. The model used in this study to estimate the response surface is the quadratic polynomial represented by the following equation:

$$Y = \beta_0 + \sum_{i=1}^n \beta_i x_i + \sum_{i=1}^{n-1} \sum_{j=i+1}^n \beta_{ij} x_i x_j + \sum_{i=1}^n \beta_{ii} x_i^2 \quad (2)$$

where Y is the dye percentage removal, n is the number of factors, β_0 is the intercept term, β_i , β_{ij} and β_{ii} are the linear, interactive and quadratic coefficients, respectively. x_i 's are the levels of the independent variables (factors) under study.

The statistical software Design-Expert 6.0.7 (Stat-Ease Inc., Minneapolis, USA) was used for design of experiments, regression and graphical analyses of the data obtained, and statistical analysis of the model to evaluate the analysis of variance (ANOVA).

2.7. Preparation of TiO₂ nanoparticles

TiO₂ nanoparticles were prepared according to Jiang et al. [13], by sol–gel method from TiCl₄ with ammonia solution as precipitating agent and ethanol as dispersing agent; 25 mL TiCl₄ were dissolved in 20 mL distilled water in an ice-water bath. The titanium solution was then slowly mixed with 30 mL distilled water and 20 mL ethanol, and ammonia was added drop wise until pH 9. During the ammoniac addition, an intensive precipitation occurred. After the solvent was evaporated at 80°C for 24 h, the precipitates were dried at 300°C for 2 h to remove excess NH₄Cl and then calcined at 600°C in an air stream.

The prepared TiO₂ nanoparticles were characterized by transmission electron microscopy (TEM, Jeol

Jem 2100F, 80–200 kV, Japan) and high-resolution X-ray diffractometer (XRD; PANalytical XPERT PRO MPD, Netherland) coupled with Cu α radiation source ($\lambda = 1.5418 \text{ \AA}$) operated at 40 kV and 40 mA. The diffraction patterns were recorded at room temperature in the angular range of $4\text{--}70^\circ (2\theta)$ with step size $0.02^\circ (2\theta)$ and scan step time 0.5 (s). The crystalline phases were identified using Joint Committee on Powder Diffraction Standards (JCPDS). The crystallite size, D_{XRD} , was calculated according to Scherer's equation [14]. Specific surface area was determined by BET method.

2.8. Biosorbent regeneration

The separated biomass with adsorbed dye was re-suspended in 20 mL distilled water and the pH was adjusted to 9 with 10% NaOH solution. After stirring at room temperature for 20 min, most of the adsorbed dye was desorbed. The biomass was then separated from the solution by centrifugation at 2,000 rpm for 15 min. The supernatant containing the desorbed dye was then neutralized by 1 M HCl and was used in the next photo-degradation experiment. The separated biomass was washed with 1 M HCl and then distilled water until the pH of decanted water become 7. The regenerated biomass was then used in the next adsorption experiment.

2.9. Photo-degradation of RR-84

The photo-catalytic reaction was carried out in a cylindrical Pyrex reactor, containing 20 mL of the dye solution with 1 g/L TiO_2 on a magnetic stirrer set at 500 rpm to maintain the photo-catalyst in suspension. The suspension was irradiated with UV 254 nm (8 W) lamp. All experiments were performed at $25 \pm 1^\circ\text{C}$. Samples were collected at prescribed time intervals to determine photo-degradation rate of the dye by measuring the absorbance at λ_{max} 485 nm.

3. Results and discussion

3.1. Elucidation and validation of regression model

The objectives of the data analysis were to fit a regression model equation, specify regression coefficients and recognize the significant model terms, and finally determine the factors optimum levels which would lead to a maximum response, i.e. maximum percentage of dye removal. Using the obtained experimental results, a second-order polynomial regression model equation relating the dye removal efficiency

and process parameters was developed and represented as follows:

$$Y = 41.58 + 2.52A + 3.23B - 1.43C - 1.44D + 9.04E - 1.58A^2 + 0.86B^2 + 0.54C^2 + 1.91D^2 - 0.84E^2 - 1.4AB + 0.68AC + 0.11AD + 0.59AE - 0.73BC + 1.16BD - 1.84BE + 1.52CD + 0.072CE - 0.91DE \quad (3)$$

where positive sign in front of the terms indicate synergetic effect, whereas negative sign indicates antagonistic effect.

Table 2 illustrates the statistical combinations of variables with the experimental and predicted response values.

It was observed that the percentage dye removal increased with increase of adsorbent dosage. This may be due to the increase in the available active surface sites of the adsorbent, i.e. increase in active surface area. But the biosorption percent decreased with increase in the initial dye concentration due to the saturation of sorption sites on biosorbent. The increase in mixing rate increased to some extent the dye uptake, indicating more effective contact between biomass and dye solution at higher mixing rate (100 rpm). The adsorption of RR-84 on spent waste biomass of *S. cerevisiae* decreased by increasing the temperature of the solution from 15 to 35°C , therefore, this system is exothermic, in which there is only physical adsorption [15,16]. Ong et al. [17] reported that a boundary layer is surrounding the biomass and a decrease in its effect is observed with increasing the mixing rate.

The validity of the fitted model was evaluated and its statistical significance was controlled by *F*-test. The ANOVA for the response surface full quadratic model is given in Table 3. It can be indicated that the model is highly statistically significant at 95% confidence level, with *F*-value of 15.02 and very low probability *p*-value of <0.0001 , i.e. there is less than 0.01% chance that this error is caused by noise. The values of the determination coefficients, R^2 and R^2_{adj} which measure the model fitting reliability for model (Eq. (3)), were calculated to be 0.9120 and 0.8519, respectively. This suggests that approximately 91.2% of the variance is attributed to the variables and indicated a high significance of the model. Thus, only 8.8% of the total variations cannot be explained by the model which ensures the good adjustment of the above model to experimental data. Confirmation of the adequacy of the regression model was reflected also by the good agreement between experimental and predicted values of response variables as shown in Table 2. Where, the actual experimental biosorption percentage ranged

Table 2
Full factorial CCD matrix for RR-84 removal

Run number	A mixing rate, rpm	B time, h	C temperature, °C	D initial dye concentration, mg/L	E biosorbent dosage % (w/v)	Dye removal %	
						Experimental	Predicted
1	-1	-1	+1	-1	+1	43.15	46.77
2	-1	-1	+1	+1	-1	21.59	22.94
3	-1	0	0	0	0	38.56	37.48
4	0	0	0	0	0	41.00	41.58
5	+1	+1	0	+1	+1	56.27	53.79
6	0	+1	0	0	0	45.80	45.66
7	0	0	0	0	0	41.00	41.58
8	-1	-1	-1	-1	+1	50.60	52.41
9	-1	-1	+1	+1	+1	43.00	42.55
10	-1	-1	-1	+1	-1	26.48	22.80
11	-1	+1	-1	-1	-1	40.11	41.52
12	+1	+1	-1	-1	+1	62.74	58.99
13	+1	+1	+1	+1	-1	46.56	39.36
14	-1	-1	+1	-1	-1	24.33	23.51
15	0	0	0	0	+1	48.90	50.14
16	+1	+1	-1	+1	-1	37.54	39.43
17	+1	-1	+1	-1	+1	59.96	56.94
18	+1	0	0	0	0	43.37	42.52
19	+1	-1	-1	+1	+1	46.41	50.03
20	0	0	0	0	-1	34.50	31.33
21	+1	+1	+1	-1	-1	36.43	34.84
22	-1	+1	-1	-1	+1	53.05	57.15
23	0	0	+1	0	0	40.98	40.69
24	+1	-1	-1	-1	+1	62.31	59.86
25	0	0	0	-1	0	46.90	44.93
26	+1	-1	+1	+1	+1	57.78	53.17
27	+1	-1	+1	-1	-1	28.12	31.30
28	0	0	0	0	0	41.00	41.58
29	+1	+1	+1	-1	+1	46.93	53.13
30	+1	-1	+1	+1	-1	29.88	31.19
31	-1	+1	+1	+1	+1	50.88	48.98
32	-1	-1	-1	-1	-1	31.60	29.44
33	0	0	0	0	0	41.00	41.58
34	0	0	0	+1	0	42.00	42.05
35	-1	+1	+1	+1	-1	31.40	36.72
36	0	0	0	0	0	37.92	41.58
37	0	-1	0	0	0	41.00	39.21
38	+1	+1	-1	-1	-1	39.85	40.98
39	-1	-1	-1	+1	+1	40.84	42.12
40	0	0	0	0	0	41.00	41.58
41	-1	+1	+1	-1	+1	55.18	48.57
42	0	0	0	0	0	41.00	41.58
43	-1	+1	-1	+1	+1	53.90	51.49
44	-1	+1	-1	+1	-1	39.00	39.52
45	+1	-1	-1	-1	-1	33.28	34.51
46	0	0	0	0	0	41.00	41.58
47	-1	+1	+1	-1	-1	32.95	32.65
48	+1	+1	+1	+1	+1	48.18	54.00
49	+1	-1	-1	+1	-1	26.76	28.33
50	0	0	-1	0	0	45.18	43.55

Table 3
ANOVA of the fitted quadratic regression model Eq. (3)

Source	SS*	df*	MS*	F-value	p-value	Remarks
Model	4,097.15	20	204.86	15.02	<0.0001	Highly significant
A	216.27	1	216.27	15.86	0.0004	Highly significant
B	353.81	1	353.81	25.94	<0.0001	Highly Significant
C	69.53	1	69.53	5.10	0.0317	Significant
D	70.68	1	70.68	5.18	0.0304	Significant
E	3,006.12	1	3,006.12	220.41	<0.0001	Highly Significant
A ²	6.14	1	6.14	0.45	0.5075	Non significant
B ²	1.83	1	1.83	0.13	0.7171	Non significant
C ²	0.72	1	0.72	0.053	0.8200	Non significant
D ²	9.01	1	9.01	0.66	0.4229	Non significant
E ²	1.75	1	1.75	0.13	0.7229	Non significant
AB	62.94	1	62.94	4.62	0.0402	Significant
AC	14.82	1	14.82	1.09	0.3058	Non significant
AD	0.41	1	0.41	0.030	0.8629	Non significant
AE	11.31	1	11.31	0.83	0.3701	Non significant
BC	17.23	1	17.23	1.26	0.2703	Non significant
BD	43.01	1	43.01	3.15	0.0863	Possibly significant
BE	107.75	1	107.75	7.90	0.0088	Significant
CD	73.69	1	73.69	5.40	0.0273	Significant
CE	0.17	1	0.17	0.012	0.9131	Non significant
DE	26.64	1	26.64	1.95	0.1728	Non significant
Residual	395.53	29	13.64			
Corrected total	4,492.68	49				

*SS: sum of squares, df: degree of freedom, MS: mean square.

from 21.59 to 62.53% and its corresponding predicted values are 22.94 and 59.43%, respectively. "Adeq Precision" measures the signal to noise ratio. A ratio >4 is desirable. The ratio of 14.483 indicated an adequate signal. This model is reliable and can be used to navigate the design space.

The relationship between predicted and experimental values of biosorption efficiency (% dye removal) is shown in Fig. 2(a). It can be seen that there is a high correlation ($R^2 = 0.9091$) between the predicted and experimental values indicating that the predicted and experimental values were in reasonable agreement. It means that the data fit well with the model and give a convincingly good estimate of response for the system in the experimental range studied.

Fig. 2(b) shows the normal probability plots of the standardized residuals for biosorption efficiency. A normal probability plot indicates if the residuals follow a normal distribution, in which case the points will follow a straight line. Since some scattering is expected even with the normal data, as shown in Fig. 2(b), it can be assumed that the data are normally distributed. Thus, it indicates a good validity for the approximation of the quadratic regression model.

Fig. 2(c) shows standardized residual vs. predicted values for percentage dye removal. In this research, points of observed runs were scattered randomly within the constant range of residuals across the graph. Thus, it revealed no obvious pattern and unusual structure, i.e. the model is adequate and there is no reason to suspect any violation of the independence or constant variance assumption in all runs. The standardized residuals vs. run plot represented in Fig. 2(d) shows randomly scattered points ranged between ± 2.5 ; the errors were normally distributed and insignificant.

ANOVA was also applied to establish the statistical significance of the model parameters at 95% confidence level. The significance of each coefficient was determined by *F*-values and *p*-values (Table 3). The larger the magnitude of the *F*-value and the smaller the *p*-values, the more significant is the corresponding coefficient. This implies that the variables with the largest effect (i.e. highly significant) were: the linear effect of mixing rate, incubation period and biomass dosage followed by process temperature and initial dye concentration (i.e. significant). The interactive effect of incubation period and biomass dosage has higher significant effect than the interactive effect of

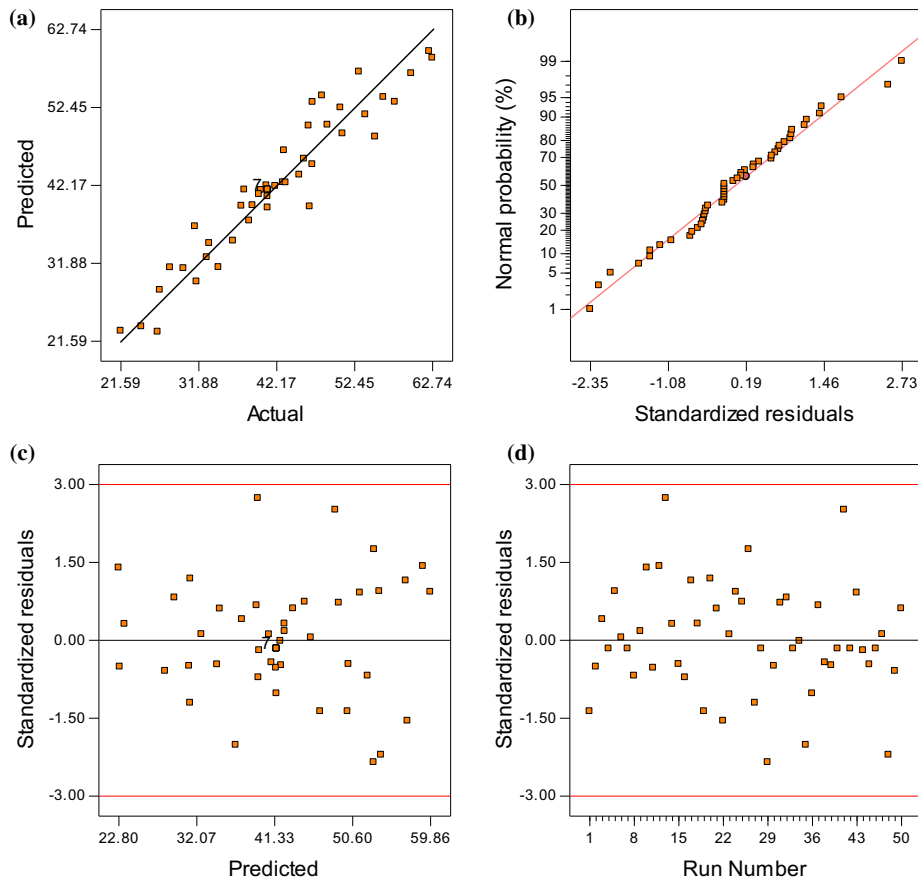


Fig. 2. Validation of model. (a) Experimental values vs. predicted values for the model. (b) Normal probability plot of the residuals. (c) Diagnostic plot for biosorption, residual vs. predicted. (d) Diagnostic plot for biosorption, residual vs. run.

process temperature and initial dye concentration, mixing rate and incubation period, while incubation period and initial dye concentration have a lower interactive effect.

The perturbation plot Fig. 3 shows the comparative effects of all independent variables on percentage dye removal (biosorption efficiency). The curvatures show the positive synergetic effect of independent variables can be ranked in the following decreasing order biomass dosage > incubation period > mixing rate. But the antagonistic effects of process temperature and initial dye concentration on biosorption process are nearly the same.

3.2. Response surface optimization of the biosorption process

Three-dimensional response surface graphical diagrams of the regression Eq. (3) were plotted to understand the interactive relationship between the independent variables and percentage dye removal

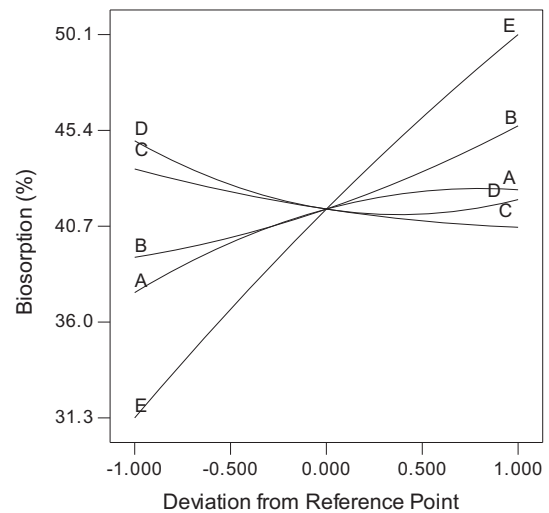


Fig. 3. Perturbation plot for percentage dye removal.

(i.e. biosorption %) and to determine the optimum conditions for maximum dye removal.

Fig. 4(a) represents the effect of mixing rate rpm and incubation period h on biosorption process at constant process temperature, initial dye concentration and biomass dosage of 15°C, 100 mg/L and 0.6%, respectively. The biosorption percentage increased with increase of incubation period and mixing rate, recording approximately 60% dye removal within incubation period of 13–20 h and mixing rate of 30–100 rpm. Fig. 4(b) represents the effect of mixing rate rpm and process temperature °C on dye removal at constant incubation period, initial dye concentration and biomass dosage of 20 h, 100 mg/L and 0.6%, respectively. It is obvious from Fig. 4(b) that biosorption percentage decreased with increase in temperature but increased with increase in mixing rate, recording maximum dye removal of ≈60% at 15°C and 100 rpm. Fig. 4(c) represents the interactive effect of mixing rate rpm and initial dye concentration mg/L on dye removal at constant incubation period, process temperature and biomass dosage of 20 h, 15°C and 0.6%, respectively. The biosorption percentage

decreased with increase in dye concentration but increased with increase in mixing rate, recording maximum dye removal of ≈60% at 100 mg/L and 100 rpm. Fig. 4(d) represents the interactive effect of mixing rate rpm and biomass dosage (wt%, w/v) on biosorption percentage at constant incubation period, process temperature and initial dye concentration of 20 h, 15°C and 100 mg/L, respectively. The biosorption percentage increased with increase of both mixing rate and biomass dosage, recording maximum dye removal of ≈60% at 100 rpm and 0.6%.

3.3. Optimization of biosorption process

The optimization process was carried out to determine the optimum value of maximum percentage of dye removal (biosorption %), using the Design-Expert 6.0.7 software. According to the software optimization step, the desired goal for each operational condition (A mixing rate, B incubation period, C process temperature, D initial dye concentration and E biomass dosage)

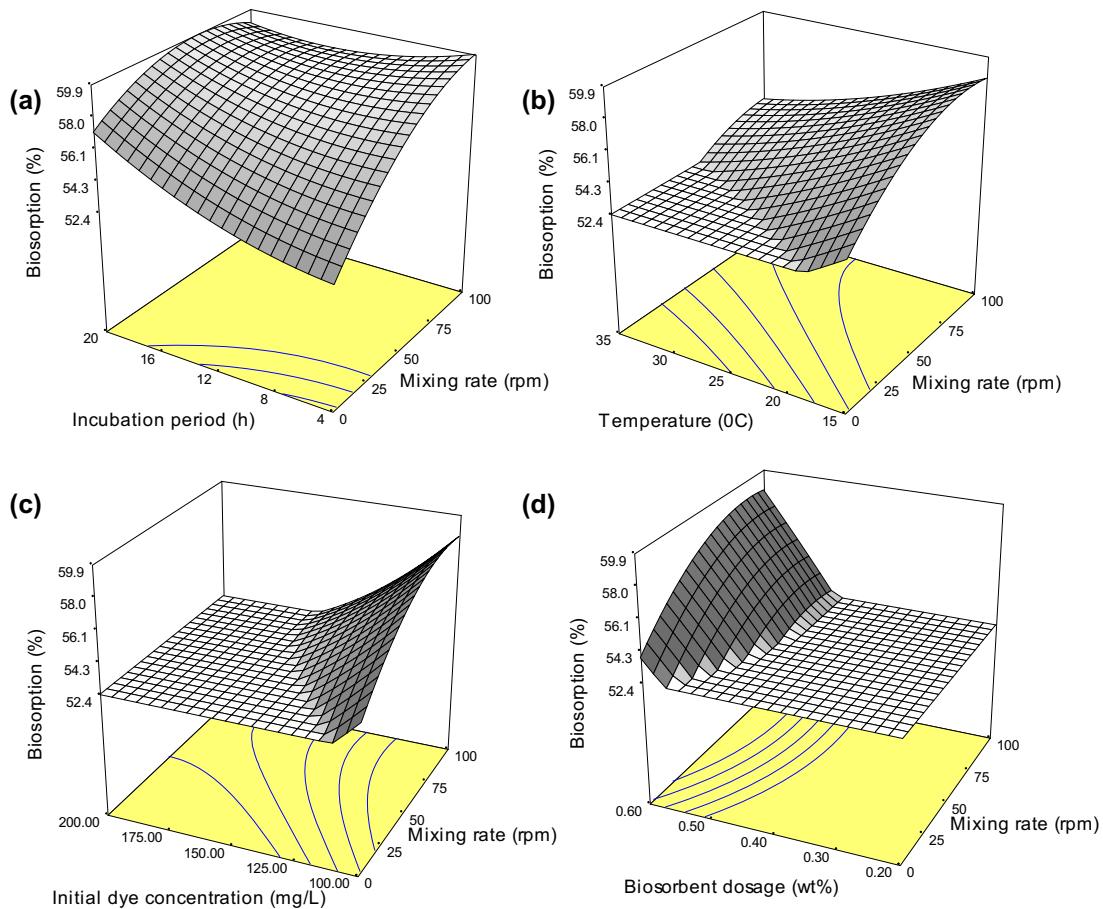


Fig. 4. Response surface plots of biosorption process.

was chosen “within” the studied range. The response (biosorption percentage) was defined as maximum to achieve the highest performance. The program combines the individual desirability into a single number, and then searches to optimize this function based on the response goal. Accordingly, the optimum working conditions and respective biosorption percentage were established. The optimum working conditions with respective predicted biosorption percentage are presented in Table 4. This was in agreement with RSM optimization: 30–100 rpm, 13–20 h, 15°C, 100 mg/L and 0.6%, respectively.

3.4. Characterization of prepared TiO₂

It is known that there are three polymorphs of titania: anatase, rutile and brookite. Among the three, anatase TiO₂ has the highest photocatalytic activity. The XRD pattern of the prepared TiO₂ particles (Fig. 5) shows two TiO₂ phases; anatase and rutile were formed and that all the peaks are in good agreement with the standard spectrum (JCPDS No. 01-075-2246, 00-034-0180 for anatase and rutile, respectively). The average crystallite sizes (D_{XRD}) of TiO₂ nanoparticles, calculated from XRD pattern were found to be 16.6 and 17.3 nm for anatase and rutile, respectively. The anatase to rutile phase ratio was 95:5 and the S_{BET} was 54 m²/g. It is obvious from TEM image Fig. 6 that TiO₂ existed as nanoparticles of average sizes, 6–15 nm, which is approximately in agreement with that of XRD measurements.

3.5. Regeneration and reuse of biosorbent

After the performance of biosorption batch process at selected optimum conditions, 100 mg/L initial dye concentration, 0.6 wt% biomass dosage, 90 rpm mixing rate, 13 h incubation period and 15°C process temperature, maximum biosorption percentage of 62% with biosorption capacity of 51.67 mg/g was achieved. Regeneration of adsorbent would make the biosorption process economical. The percentage of desorption increased with increase of pH of aqueous solution, reaching its maximum value (>95%) at pH 9. The functional groups on

the surface of spent waste biomass of *S. cerevisiae* are carboxyl, hydroxyl and amide. The surface of yeast would become negatively charged at high solution pH, thus increasing the electrostatic repulsive force between the reactive dye and the biomass. The biosorbent was easily separated by centrifugation, washed and reused in the next cycle of adsorption experiment.

When applying the regenerated biomass for removal of the remaining dye from the first batch, approximately complete dye removal occurred of ≈97% with biosorption capacity of 30.83 mg/g.

Upon applying, the regenerated biomass for new four successive adsorption–desorption cycles of new batches with initial dye concentration of 100 mg/L, biosorption percentage recorded, 62, 61.5, 50 and 36% with biosorption capacity of 51.62, 51.25, 41.67 and 30 mg/g, respectively.

3.6. Photo-degradation of desorbed RR-84 with TiO₂ nanoparticles

The pseudo-first-order kinetic equation (Eq. (4)) was applied to determine the photo-degradation rate of the collected desorbed dye solution in a UV/TiO₂ process. Two batch processes were done with initial dye concentrations of 95 and 135 mg/L; the obtained concentrated output solutions of one cycle and four successive cycles of the previous biosorption–desorption batches. The dye was gradually degraded, recording ≈96.85 and 86.67% after 120 min, respectively.

$$\ln \left(\frac{C_0}{C_t} \right) = K_{\text{obs}} t \quad (4)$$

where C_0 and C_t denote the RR-84 concentrations at $t = 0$ and $t = t$, respectively, where K_{obs} is the apparent pseudo-first-order rate constant and the variation of the dye concentration influences directly to this constant.

The K_{obs} values were obtained from the slope in the linear regression analysis of the concentration curves, where it decreased with the increase of initial dye concentration, recording 0.0745 min⁻¹ (R^2 0.9516) and 0.0323 min⁻¹ (R^2 0.9558), respectively.

Table 4
Optimum conditions solutions for RR-84 biosorption by spent waste biomass of *S. cerevisiae*

Number of trials	Factors					Desirability	Biosorption %	
	A, rpm	B, h	C, °C	D, mg/L	E, wt%		Predicted	Experimental
1	30.51	20.00	15.00	100.00	0.59	0.904	58.8	62
2	90.67	13.33	15.00	100.05	0.60	0.901	58.7	62

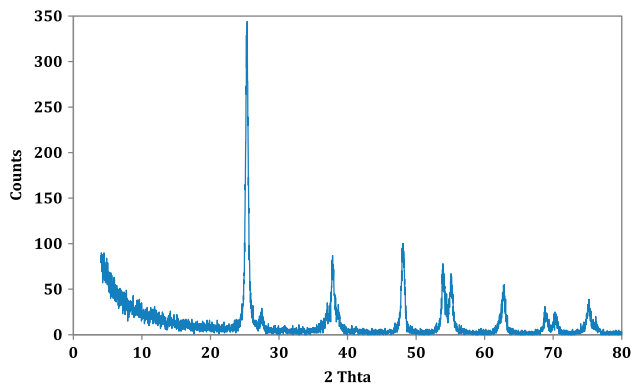


Fig. 5. XRD patterns of the prepared TiO₂ particles.

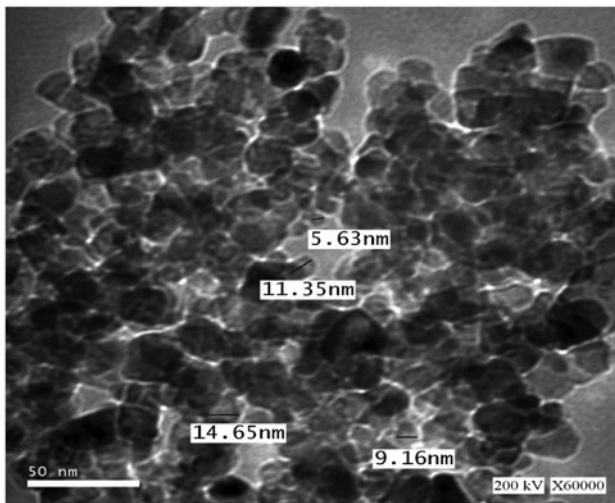
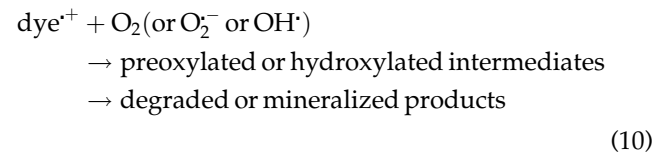
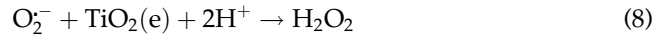
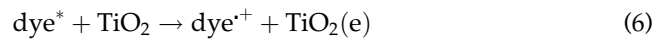


Fig. 6. TEM images of the prepared TiO₂ particles.

When a semiconductor such as TiO₂ absorbs a photon with energy equal to or greater than its band gap width (3.2 eV), an electron may be promoted from the valence band to the conduction band (e^-_{cb}) leaving behind an electron vacancy in the valence band (h^+_{vb}) [18]. The holes at the TiO₂ valence band, having an oxidation potential of +2.6 V, can oxidize water or hydroxide to produce hydroxyl radicals. The hydroxyl radical is a powerful oxidizing agent and enables a non-specific attack on organic compounds; under favorable conditions the final photoproducts are H₂O and CO₂ and inorganic anions. The general possible detailed mechanism of dye degradation upon irradiation is described by Eqs. (5)–(10) [4,18]:



The reason for the decrease of photo-degradation efficiency with increase of initial dye concentration might be presumed that in high dye concentrations, the production of hydroxyl radicals on the surface of catalyst was reduced since the active sites were occupied by dye molecules. Another possible reason for these results is the effect of UV screening of the own dye. In high dye concentrations a major amount of UV is apt to be absorbed by dye molecules proportional to OH particles and this reduces the efficiency of the catalytic reaction due to the decline in the active O₂⁻ and OH[·] concentrations [19]. Moreover, the reduction of the light path length as the concentration and deepness of the colour of the solution rises cannot be also neglected. Another possible reason is the intervention of the by-products formed during the degradation process [20].

4. Conclusion

This study proved that factorial design analysis based on central composite design CCD of experiments and RSM are reliable and powerful tools for modelling, optimizing and studying the interactive effects of five important parameters (mixing rate, incubation period, process temperature, initial dye concentration and biosorbent dosage) in a batch biosorption process for Reactive Red-88 dye removal using spent waste biomass of *S. cerevisiae*, with maximum adsorption capacity of 51.67 mg/g and percentage dye removal of ≈62%.

The experiments showed that integration of the biosorption with photo-catalytic oxidation using TiO₂ nanoparticles would be beneficial for practical applications. First, the contaminants were removed effectively from aqueous effluents by readily available, low cost biosorbent, then the dye was desorbed by simple optimization of pH and finally, the desorbed dye was photo-degraded by TiO₂ nanoparticles under UV-illumination, for complete mineralization of the

contaminant. The regenerated biomass and photo-catalyst can be used for several cycles.

The changes occurred on the biomass surface after regeneration is going to be investigated thoroughly in further studies. Also, more details about photo-degradation mechanism and optimization process are needed to be investigated.

References

- [1] J.S. Chang, C. Chou, Y.C. Lin, P.J. Lin, J.Y. Ho, T. Lee Hu, Kinetic characteristics of bacterial azo-dye decolorization by *Pseudomonas luteola*, *Water Res.* 35 (2001) 2841–2850.
- [2] Y. Safa, H.N. Bhatti, Biosorption of Direct Red-31 and Direct Orange-26 dyes by rice husk: Application of factorial design analysis, *Chem. Eng. Res. Des.* 89(12) (2011) 2566–2574.
- [3] Z. Zainal, L.K. Hui, M.Z. Hussein, Y.H. Taufiq-Yap, A.H. Abdullah, I. Ramli, Removal of dyes using immobilized titanium dioxide illuminated by fluorescent lamps, *J. Hazard. Mater.* 125 (2005) 113–120.
- [4] R. Xu, J. Li, J. Wang, X. Wang, B. Liu, B. Wang, X. Luan, X. Zhang, Photocatalytic degradation of organic dyes under solar light irradiation combined with Er^{+3} : YAlO_3/Fe - and Co-doped TiO_2 coated composites, *Sol. Energy Mater. Sol. Cells* 94(6) (2010) 1157–1165.
- [5] L. Andronic, A. Enesca, C. Vladuta, A. Duta, Photocatalytic activity of cadmium doped TiO_2 films for photocatalytic degradation of dyes, *Chem. Eng. J.* 152(1) (2009) 64–71.
- [6] A. Giwa, P.O. Nkeonye, K.A. Bello, E.G. Kolawole, A.M.F. Oliveira, Campos, solar photo-catalytic degradation of Reactive Yellow 81 and Reactive Violet 1 in aqueous solution containing semiconductor oxides, *Int. J. Appl. Sci. Technol.* 2(4) (2012) 90–105.
- [7] Y. Wang, Solar photocatalytic degradation of eight commercial dyes in TiO_2 suspension, *Water Res.* 34(3) (2000) 990–994.
- [8] T.V.N. Padmesh, K. Vijayaraghavan, G. Sekaran, M. Velan, Batch and column studies on biosorption of acid dyes on fresh water macro alga *Azolla filiculoides*, *J. Hazard. Mater.* 125 (2005) 121–129.
- [9] J.Y. Farah, N.Sh. El-Gendy, L.A. Farahat, Biosorption of Astrazone Blue basic dye from an aqueous solution using dried biomass of Baker's yeast, *J. Hazard. Mater.* 148 (2007) 402–408.
- [10] J. Yu, R. Chi, X. Su, Z. He, Y. Qi, Y. Zhang, Desorption behavior of methylene blue on pyromellitic dianhydride modified biosorbent by a novel eluent: Acid TiO_2 hydrosyl, *J. Hazard. Mater.* 177 (2010) 222–227.
- [11] K. Vijayaraghavan, Y.S. Yun, Chemical modification and immobilization of *Corynebacterium glutamicum* for biosorption of Reactive Black 5 from aqueous solution, *Ind. Eng. Chem. Res.* 46 (2007) 608–617.
- [12] K. Vijayaraghavan, S.W. Won, J. Mao, Y.S. Yun, Chemical modification of *Corynebacterium glutamicum* to improve methylene blue biosorption, *Chem. Eng. J.* 145 (2008) 1–6.
- [13] X. Jiang, G. Ding, L. Lou, Y. Chen, X. Zheng, Effect of ZrO_2 addition on CuO/TiO_2 activity in the $\text{NO}+\text{CO}$ reaction, *Catal. Today* 93–95 (2004) 811–818.
- [14] H.G. Yang, H.C. Zeng, Preparation of hollow anatase TiO_2 nanospheres via Ostwald ripening, *J. Phys. Chem. B* 108 (2004) 3492–3495.
- [15] A. Dabrowski, Adsorption from theory to practice, *Adv. Colloid Interface Sci.* 93(1–3) (2001) 135–224.
- [16] D. Schimmel, K.C. Fagnani, J.B. Santos, M.A.S.D. Barros, E. Silva, Adsorption of Turquoise Blue QG reactive dye on commercial activated carbon in batch reactor: Kinetic and equilibrium studies, *Braz. J. Chem. Eng.* 27(2) (2010) 289–298.
- [17] S.T. Ong, C.K. Lee, Z. Zainal, Removal of basic and reactive dyes using ethylene diamine modified rice hull, *Bioresour. Technol.* 98 (2009) 2792–2799.
- [18] M.A. Tariq, M. Faisal, M. Saquib, M. Muneer, Heterogeneous photocatalytic degradation of an anthraquinone and a triphenylmethane dye derivative in aqueous suspensions of semiconductor, *Dyes Pigm.* 76 (2) (2008) 358–365.
- [19] I.K. Konstantinou, T.A. Albanis, TiO_2 -assisted photocatalytic degradation of azo dyes in aqueous solution: Kinetic and mechanistic investigations, *Appl. Catal., B* 49(1) (2004) 1–14.
- [20] A. Giwa, P.O. Nkeonye, K.A. Bello, E.G. Kolawole, Solar photo-catalytic degradation of Acid Blue 29, *J. Chem. Soc. Niger.* 36(1) (2011) 82–89.